ferent evolutionary models (*1*), and over 100 maximum-likelihood trees were run in the course of this study.
37. Z. Yang, *Mol. Biol. Evol.* **10**, 1396 (1993).
38. D. L. Swofford, PAUP*. Phylogenetic Analysis Using Parsimony (*and Other Methods) (Sinauer, Sunderland, MA, 1999).
39. We also tested other aspects of our evolutionary model. We found that the assignment of base frequencies by means of the phylogenetic trees gave consistently better results than empirical base frequencies. The REV model performed better than an F84 model (*2*), which only includes rate parameters for transitions and transversions instead of for each pair of bases. Also, for the envelope gene analyses, the improvement in the log-likelihood scores comparing the REV model with a uniform rate of evolution at all sites, to the REV model with rate variation at different sites estimated by the maximum-likelihood method, was many times larger than the number of positions (*1*), justifying the increase in parameters (*3*).
40. B. Korber, P. Sharp, D. Ho, *Nature* **400**, 326 (1999); J. Goudsmit and V. Lukoshov, *Nature* **400**, 325 (1999).
41. B. Korber *et al.*, data not shown.
42. V. Courgnaud *et al.*, *Virology* **247**, 41 (1998).
43. Y. Wangroongsarb *et al.*, *Southeast Asian J. Trop. Med. Public Health* **16**, 517 (1985); D. Smith, *Lancet* **335**, 781 (1990); C. Mason *et al.*, *J. Acquir. Immune Defic. Syndr. Hum. Retrovirol.* **19**, 165 (1996); R. Bunnell *et al.*, *AIDS* **13**, 509 (1999).
44. C. Kuiken *et al.*, *Am. J. Epidemiol.*, in press.
45. F. McCutchan *et al.*, *J. Virol.* **70**, 3331 (1996); S. Subbarao *et al.*, *AIDS Res. Human Retroviruses* **14**, 319 (1998).
46. F. Gao *et al.*, *J. Virol.* **70**, 7013 (1996); J. K. Carr *et al.*, *J. Virol.* **70**, 5935 (1996).
47. M. S. Gottlieb *et al.*, *N. Engl. J. Med.* **305**, 1425 (1981); M. S. Gottlieb *et al.*, *Morb. Mortal. Wkly. Rep.* **30**, 250 (1981).
48. R. Selik, H. Haverkos, J. Curran, *Am. J. Med.* **76**, 493 (1984); J. Pape, *N. Engl. J. Med.* **309**, 945 (1983); L. Gazzolo, *N. Engl. J. Med.* **311**, 1252 (1984).
49. E. Hooper. *The River* (Little, Brown, Boston, 1999). See pp. 77–82 and 440–443 for discussion of early cases in the United States and Haiti, and pp. 550, 791, and 1009 for a discussion of the number of primate kidneys required to make OPV.
50. S. Chevret *et al.*, *J. Epidemiol. Commun. Health* **46**, 582 (1992).
51. W.-H. Li, M. Tanimura, P. Sharp, *Mol. Biol. Evol.* **5**, 313 (1988); T. Gojobori *et al.*, *Proc. Natl. Acad. Sci. U.S.A.* **340**, 1605, 4108 (1990); J. Kelly, *Genet. Res.* **64**, 1, 1994.
52. K. Liitsola *et al.*, *AIDS* **12**, 1907 (1998).
53. A record of the ages of chimpanzees from Camp Lindi used for research noted a range from <1 to 10 years, with more than 80% less than 4 years old (S. Plotkin, personal communication; data taken from the laboratory notes of F. Deinhardt).
54. M. Grmek. *History of AIDS Emergence and Origin of a Modern Pandemic* (Princeton Univ. Press, Princeton, NJ, 1990), chaps. 10 and 15.
55. A. Chitnis, D. Rawls, J. Moore, *AIDS Res. Hum. Retroviruses* **16**, 5 (2000).
56. We thank D. Pollock, T. Leitner, and B. Bruno for suggestions concerning phylogenetics, maximum likelihood, and estimating the error on time of sampling; G. Shaw for suggesting the 1959 control; S. Wain-Hobson and G. Myers for clarifying discussions on the interpretation and limitations of these results; B. Foley and C. Kuiken for numerous helpful discussions; and K. Rock and J. Shepard for technical support. G. Olsen and J. Thorne generously supplied source code and helped us interpret their work. The research of the Los Alamos authors was supported under internal funds from the Delphi Project, S.W. and B.K. were supported by NIH (RO1-HD37356), B.K. and M.M. were supported through the Pediatric AIDS Foundation, and an anonymous foundation supplied further support for S.W. B.H.H. was supported by grants NO1 AI 85338, RO1 AI 44596, and RO1 AI 40951 from NIH.

16 December 1999; accepted 28 April 2000

Kinesin Superfamily Motor Protein KIF17 and mLin-10 in NMDA Receptor–Containing Vesicle Transport

Mitsutoshi Setou, Terunaga Nakagawa, Dae-Hyun Seog, Nobutaka Hirokawa*

Experiments with vesicles containing *N*-methyl-D-aspartate (NMDA) receptor 2B (NR2B subunit) show that they are transported along microtubules by KIF17, a neuron-specific molecular motor in neuronal dendrites. Selective transport is accomplished by direct interaction of the KIF17 tail with a PDZ domain of mLin-10 (Mint1/X11), which is a constituent of a large protein complex including mLin-2 (CASK), mLin-7 (MALS/Velis), and the NR2B subunit. This interaction, specific for a neurotransmitter receptor critically important for plasticity in the postsynaptic terminal, may be a regulatory point for synaptic plasticity and neuronal morphogenesis.

In mammalian neurons, neurotransmitter receptors such as glutamate receptors, including NMDA receptors, are sorted dynamically and precisely to the dendrites of the cell (*1*). Although putative anchoring, sorting, and signaling molecules have been colocalized with the receptors (*2*), it is not yet known how the receptors are sorted. Transport of molecules to specific regions in eukaryotic cells is accomplished by molecular motors (*3*). In neurons, various microtubule-associated motor proteins have been shown to transport organelles such as synaptic vesicle precursors and mitochondria to specific regions of the cell; however, the mechanisms by which each motor recognizes its specific cargo are not known (*3*). Here, we report that KIF17 (*4*), a neuron-specific microtubule-dependent molecular motor, binds directly and specifically to a PDZ domain (*5*) of mLin-10 (*6*) and transports the large protein complex containing the NR2B subunit, which forms the NMDA receptor with the NR1 subunit (*7*). This complex transports vesicles along microtubules in neurons such as hippocampal pyramidal neurons.

Department of Cell Biology and Anatomy, Graduate School of Medicine, University of Tokyo, Bunkyo-ku, Tokyo, Japan.

*To whom correspondence should be addressed. E-mail: hirokawa@m.u-tokyo.ac.jp

Identification of KIF17. Members of the kinesin superfamily (KIFs) support diverse transport systems in cells (*3*). We cloned KIF17, a neuron-specific motor (Fig. 1A) (*8*), to investigate the motors responsible for the sorting of various molecules within neurons. Osm-3 (*9*), a putative dendritic motor for odorant receptors in *Caenorhabditis elegans*, and KIF17 constitute a family (Fig. 1B). KIF17 is similar to Osm-3 in the head and tail domains (Fig. 1C) and has two putative stalk domains that form an α-helical coiled coil (Fig. 1D) (*10*); Osm-3, however, has only one stalk domain. Antibody raised against amino acids 505 to 707 of KIF17 (anti-KIF17) (*11*) recognized the native KIF17 protein in the brain as a single 170-kD band in SDS–polyacrylamide gel electrophoresis (PAGE) (Fig. 1E).

Although KIFs could be monomeric, homodimeric, heterotrimeric, homotetrameric, or heterotetrameric (*3*), native KIF17 has a sedimentation coefficient of 3.0 S and a Stokes radius of 170 Å, which suggests that the molecular weight of the native holoenzyme is 215 kD, about twice that calculated from the sequence of the protein (116 kD). The migration of KIF17 in native PAGE was similar to that of the recombinant full-length KIF17 protein (*12*). Thus, KIF17 probably exists as a homodimer (*13*).

To measure the direction and velocity of the KIF17 motor activity, we assayed its motility with the use of recombinant KIF17. Recombinant KIF17 could slide an axoneme toward microtubule minus-ends, indicating that KIF17 is a microtubule plus-end–directed motor (Fig. 1F). The microtubule gliding assay showed that the average speed was 0.8 to 1.2 μm/s (*14*). Thus, KIF17 can act without a coenzyme and can mediate fast intracellular transport.

KIF17 is a dendrite-specific motor protein. KIF17 appeared to be brain-specific, present in abundance in the gray matter (es-

pecially in the hippocampus) but not in white matter such as the optic nerve (Fig. 2A) (*15*). Hence, KIF17 is likely to act in the somatodendritic region of neurons rather than in the axons. Indeed, brain sections immunostained with anti-KIF17 showed KIF17 in dendrites of pyramidal neurons but not in the axons or nuclei in cerebral cortex (Fig. 2B), hippocampus (Fig. 2C), and olfactory bulb (Fig. 2D). Double staining of cultured hippocampal neurons with anti-KIF17 and an axonal marker [monoclonal antibody to phosphorylated neurofilament H (pNFH mAb)] showed that KIF17 is a dendritic motor (Fig. 2E) (*16*). The related protein Osm-3 is also known as a molecular motor localized to the dendrites of specific neurons in *C. elegans* (*9*).

KIF17 conveys a membranous cargo. To identify the cargo transported by KIF17, we investigated KIF17-associated structures by immunoisolation. The organelles purified along with KIF17 were clear membranous vesicles with a radius of 50 nm on average, as observed by electron microscopy (Fig. 3A) (*17*). These vesicles were different from those transported by KIFC2, a central nervous system–specific dendritic motor protein (*18*); nor were they identifiable as mitochondria, synaptic vesicles, dense core vesicles, or multivesicular bodies.

We then examined the association between KIF17 and the vesicles biochemically. KIF17 molecules were released from the vesicles in the presence of high salt or high pH (Fig. 3B) (*19*); this result suggests that KIF17 is peripherally associated with the membrane and should require a targeting mechanism for specific cargo vesicles.

mLin-10 is the receptor for KIF17 on the membrane. We identified adaptor molecules by yeast two-hybrid screening, using the COOH-terminal region of KIF17 (*20*). The KIF17 tail bound to a COOH-terminal PDZ domain of mLin-10, a sorting protein. The binding partner of this PDZ domain of mLin-10, which shows a very high degree of conservation from *C. elegans* to human, is unknown (*6*).

We further investigated the specificity of the binding between many KIFs and mLin-10 using mutated preys. The binding was very specific between the KIF17 tail domain and the first PDZ domain of mLin-10. Disruption of the first PDZ domain diminished the binding with KIF17, whereas disruption of the second PDZ domain or deletion of the phospholipid interaction (PI) domain did not alter the interaction (Fig. 4A). A single amino acid change or a deletion at the COOH-terminal end of KIF17 eliminated this interaction (Fig. 4B). The tails of KIF1A (400 to end), KIF1B (830 to end), KIF5A (806 to end), KIF5B (808 to end), and KIF5C (930 to end) were tested for mLin-10 binding. Only that of KIF17 bound with mLin-10.

We further examined this binding with the use of surface plasmon resonance measurement (Fig. 4C). The direct KIF17–mLin-10 interaction was confirmed to be one with strong affinity (dissociation constant K_d = 3.0×10^{-6} M). This binding was sufficiently strong to mediate sorting in vivo (*21*).

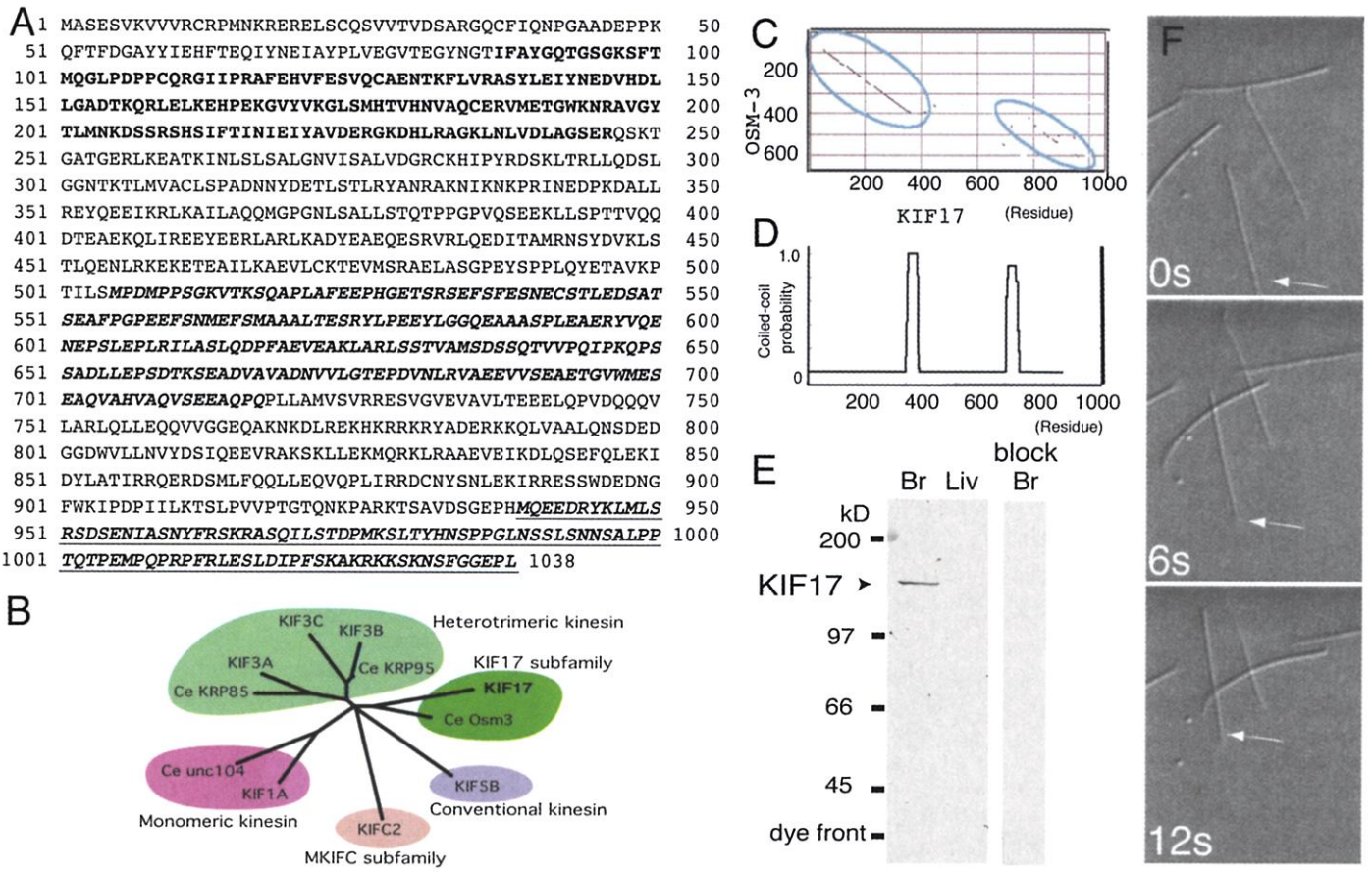

Fig. 1. Identification of KIF17 as a homodimeric microtubule-dependent motor protein. (**A**) Full-length 1038–amino acid sequence of KIF17 (the sequence has been deposited in the DDBJ/EMBL/GenBank database, accession number AB001424). The motor domain probe used to screen is indicated in boldface, the middle domain used to make antibodies is in bold italics, and the tail domain used for the two-hybrid screen is underlined. Single-letter abbreviations for amino acid residues are as follows: A, Ala; C, Cys; D, Asp; E, Glu; F, Phe; G, Gly; H, His; I, Ile; K, Lys; L, Leu; M, Met; N, Asn; P, Pro; Q, Gln; R, Arg; S, Ser; T, Thr; V, Val; W, Trp; and Y, Tyr. (**B**) Relation between KIF17 and other known KIFs, as shown by a phylogenetic tree. (**C**) Protein matrix analysis between KIF17 and Osm-3 shows similarity of their head and tail domains. (**D**) The central region of KIF17 was predicted to form two stretches of an α-helical coiled-coil structure. (**E**) Immunoblot of native KIF17. Abbreviations: Br, brain; Liv, liver; block, peptide block with recombinant KIF17 as a control. (**F**) Motility assay of recombinant KIF17 with axonemes. Arrow shows a frayed plus-end of an axoneme-microtubule bundle.

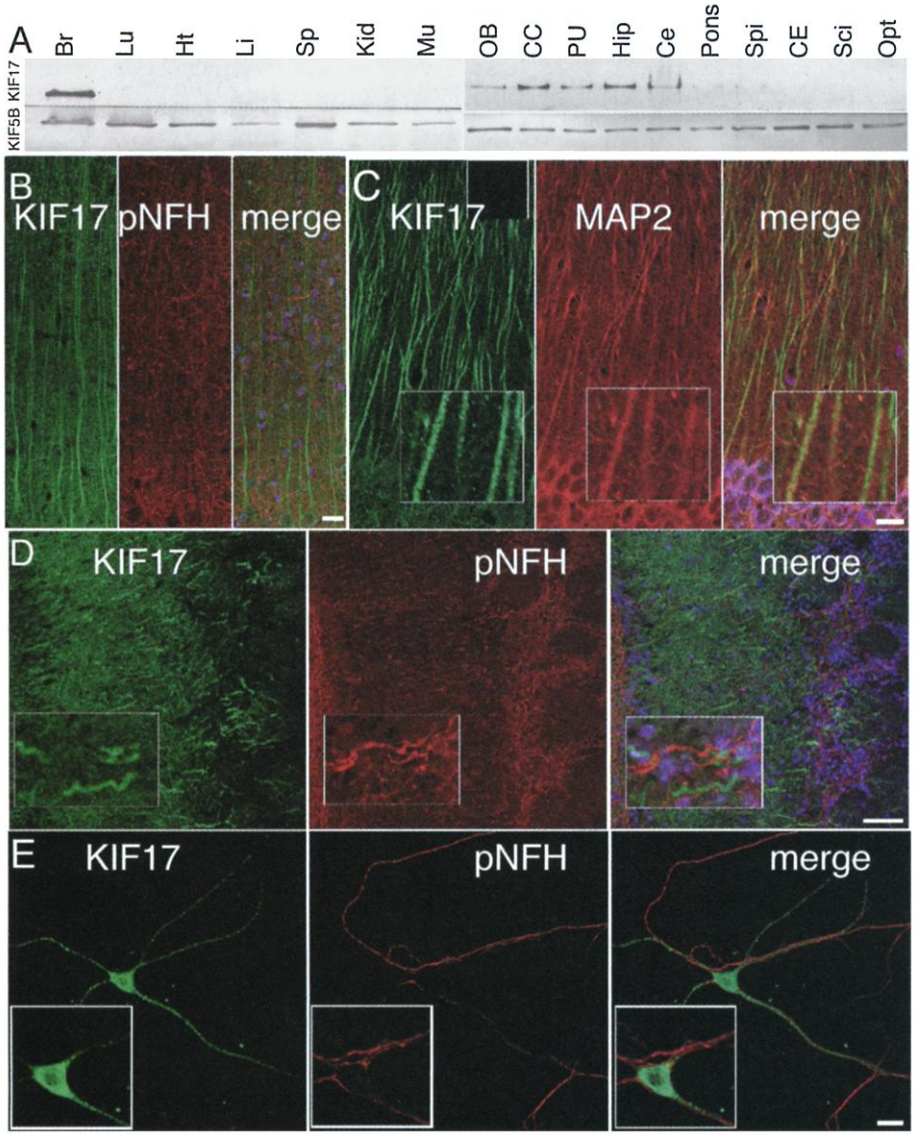

Fig. 2. Localization of KIF17 in dendrites. (**A**) KIF17 immunoblots in various tissues. Br, brain; Lu, lung; Ht, heart; Li, liver; Sp, spleen; Kid, kidney; Mu, muscle; OB, olfactory bulb; CC, cerebral cortex; PU, putamen; Hip, hippocampus; Ce, cerebellum; Spi, spinal cord; CE, cauda equina; Sci, sciatic nerve; Opt, optic nerve. KIF5B (below each lane) was used as a control. (**B**) Cerebral cortex pyramidal layer triple-stained with anti-KIF17, pNFH mAb as a marker for axons, and TOTO-3 as a marker for DNA and RNA. Scale bar, 15 μm. (**C**) Hippocampus CA3 region triple-stained by anti-KIF17, anti-MAP2 as a marker for dendrites, and TOTO-3. Scale bar, 15 μm. The peptide-blocked staining of anti-KIF17 as a negative control is shown in the small inset at the top of the KIF17 image. (**D**) Olfactory bulb mitral cell layer triple-stained with anti-KIF17, pNFH mAb, and TOTO-3. Scale bar, 50 μm. (**E**) Cultured hippocampal neuron double-stained with anti-KIF17 and pNFH mAb. Scale bar, 15 μm.

We investigated the interaction with a pull-down assay and immunoprecipitation. mLin-10 was pulled down with the recombinant KIF17, but not with KIFC2 or the tail amino acids–deleted KIF17 (Fig. 4D) (*22*). Also, mLin-10 was coimmunoprecipitated with KIF17, whereas other known KIFs (KIFC2, KIF1A, KIF3A/B, and KIF5A/B/C) were not detectable in the immunoprecipitate; this result further confirmed the specificity of the interaction (Fig. 4E) (*23*). Thus, it appears that mLin-10 is the specific binding partner of KIF17 in vivo.

NR2B sorting vesicle carried by KIF17–mLin-10 complex. In Lin-10–mutated *C. elegans*, the glutamate receptor GluR1 is mislocalized (*6*). mLin-10 exists in a protein complex with mLin-2 and mLin-7, which binds to the NMDA receptor subunit NR2B (*24*). To test whether mLin-2, mLin-7, and NR2B were cargo molecules of the KIF17–mLin-10 complex, we examined the pattern of developmental expression of the cargo proteins. The expression of the candidate proteins was concurrent with that of KIF17 (Fig. 5A), whereas conventional kinesin (KIF5B) showed a different expression pattern (*25*).

KIF17, mLin-10, mLin-2, and mLin-7 on the vesicles floated to the same low-density membranous protein fractions as NR2B, but not to other membranous protein fractions containing caveolin or mitochondrial cytochrome oxidase. Free KIF17, mLin-10, mLin-2, and mLin-7 were recovered in the heavier fractions. The ratio of free protein to membrane-bound protein increased according to the predicted binding order of the proteins to the membrane: KIF17, mLin-10, mLin-2, mLin-7, and NR2B (Fig. 5B) (*26*).

Immunoprecipitation with anti-KIF17 (*27*) was detected by antibodies to mLin-10, mLin-2, mLin-7, and NR2B, but not by antibodies to PSD-95, which binds to NR2B at the postsynaptic density (*2*) (Fig. 5C). $GABA_A$ receptor β2, glycine receptor, and substance P receptor were not detected (*28*). Immunoprecipitation with mLin-10 mAb also confirmed the interaction among KIF17, mLin-10, mLin-2, mLin-7, and NR2B (Fig. 4E). NR2B, mLin-10, mLin-2, and mLin-7 were detected in the isolated vesicles by anti-KIF17, but not by anti-KIF1A (Fig. 5C).

Fig. 3. Cargo of KIF17. (**A**) Electron micrograph of the vesicles immunoisolated with anti-KIF17. Scale bar, 20 nm. Histogram shows the vesicle count per 100 beads. (**B**) Nature of KIF17 binding to the vesicles assayed under different wash conditions (ppt, precipitant; sup, supernatant).

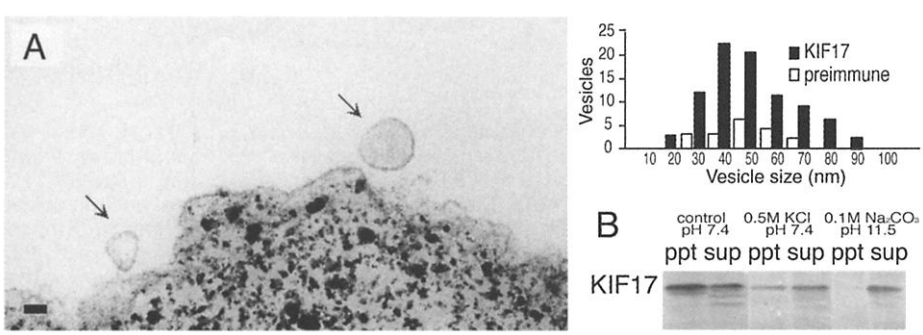

Because NR2B vesicles are transported transiently, the ratio of NR2B to other components of the complex is reduced in the immunoprecipitate. Some of the NR2B-containing vesicles attach to microtubules in a nucleotide-dependent manner, and KIF17 is located on these vesicles (Fig. 5D). This association of NR2B$^+$ vesicles to microtubules was blocked by KIF17 tail peptides fused to

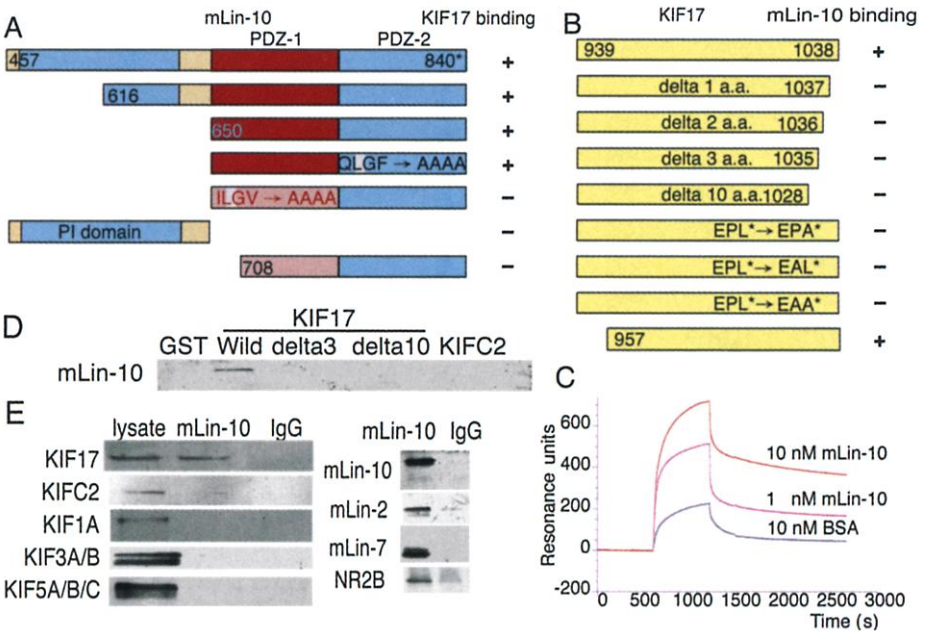

Fig. 4. Direct interaction between KIF17 tail and mLin-10 PDZ domain. (**A** and **B**) Identification of the interaction domain of KIF17 and mLin-10 using a yeast two-hybrid system. The amino acid residues of mLin-10 and KIF17 that were fused to the pLexA DNA binding domain are represented by boxes, and the corresponding amino acid positions are indicated (+, bound to KIF17 and mLin-10; –, not bound to KIF17 and mLin-10). ELGF is the known interaction consensus sequence for PDZ with the COOH-terminal of the binding partner. ILGV (residues 668 to 671 of mLin-10) → AAAA represents an ELGF motif that was mutagenized by site-directed PCR to all alanines in order to disrupt the first PDZ motif. The QLGF (residues 760 to 763 of mLin-10) → AAAA clone is another mutant with its second PDZ motif disrupted. KIF17 delta 3 a.a. denotes constructs of KIF17 with the three COOH-terminal amino acids deleted. KIF17 EPL* → EPA* denotes a construct with its wild-type COOH-terminal sequence EPL stop codon mutated to EPA stop codon. EPL* → EAL* and EPL* → EAA* are mutants constructed in the same way. (**C**) Plasmon resonance analysis of interaction of purified recombinant KIF17 with purified recombinant mLin-10 or control BSA. (**D**) Recombinant KIF17 pulls down native mLin-10 from brain lysate. Abbreviations: Wild, KIF17 939–1038; delta3, KIF17 939–1035; delta10, KIF17 939–1028; and KIFC2, KIFC2 1–423. (**E**) Immunoprecipitation of mLin-10 complex from brain.

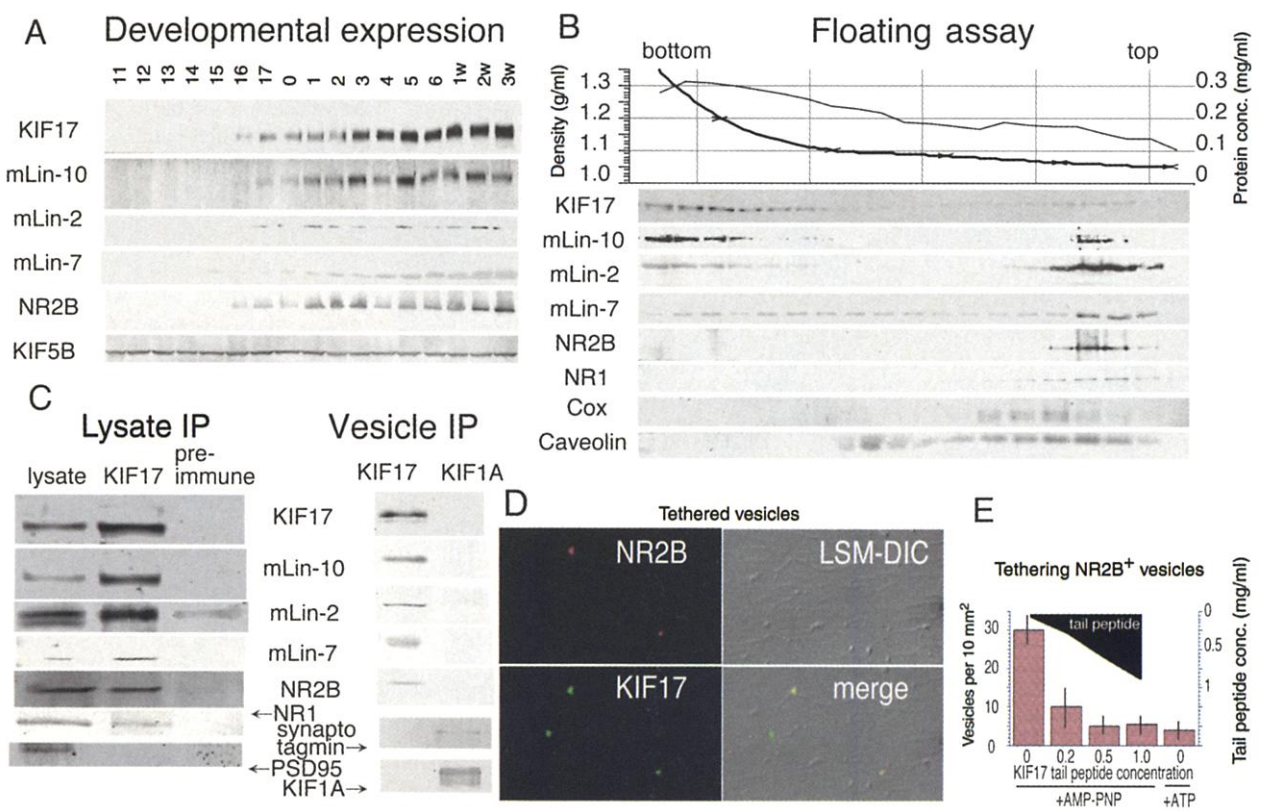

Fig. 5. KIF17–mLin-10 complex binds to NR2B-containing vesicles in a specific manner. (**A**) Developmental changes in the expression of KIF17, mLin-10, mLin-2, mLin-7, NR2B, and KIF5B in brain. Numbers above the lanes indicate embryonic days 11 to 17, postnatal days 0 to 6, and postnatal weeks 1, 2, and 3. (**B**) The Nycodenz floating assay fractions. The thick line indicates the density of the fraction; the thin line represents the protein concentration of the fraction. Cytochrome oxidase (Cox) and caveolin indicate other membranous proteins with different peaks. (**C**) Immunoprecipitation from brain lysate or vesicle fractions. (**D**) Colocalization of KIF17 and NR2B on vesicles along microtubules. Note that vesicle size and microtubule thickness are enhanced by the optical limitation of resolution. (**E**) KIF17 tail peptide block analysis. Red boxes represent numbers of NR2B$^+$ vesicles. Error bars denote SEM (n = 3).

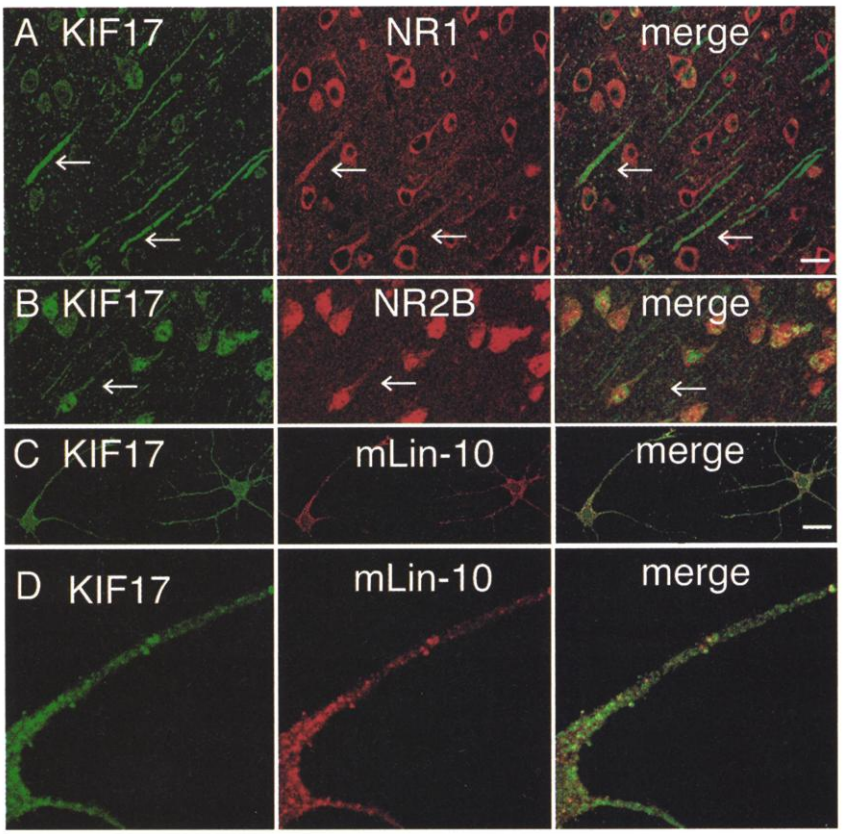

Fig. 6. KIF17 colocalizes with mLin-10, NR2B, and NR1 in dendrites of neurons. (**A**) Coronal section of cerebral cortex double-stained with anti-KIF17 and NR1 mAb. (**B**) Coronal section of cerebral cortex pepsin-treated and double-stained with anti-KIF17 and anti-NR2B (αGluRε No59). (**C** and **D**) Cultured hippocampal neuron double-stained with anti-KIF17 and anti–mLin-10. Scale bar, 15 μm.

glutathione S-transferase (GST-KIF17 939–1038) (Fig. 5E). This peptide does not block the microtubule-binding activity of the KIF17 motor domain (*14*), but binds native mLin-10 (*22*). Therefore, KIF17 tail peptide competes with the native KIF17 for mLin-10 binding and will decrease the number of NR2B-containing cargoes on the microtubules in this assay (*29*).

Thus, these proteins form a protein complex on the vesicle. We cannot exclude the possibility of another mechanism for recruitment of mLin-10 to the vesicle, but it would be reasonable to regard this mLin-10 → mLin-2 → mLin-7 → NR2B → NR1 cascade as a good candidate vesicle-binding mechanism for KIF17.

Colocalization of KIF17, mLin-10, and NR2B in the same dendrites. We immunostained brain sections and cultured hippocampal neurons. Double staining with anti-KIF17 and NR1 mab, anti-NR2B, and anti–mLin-10 revealed colocalization of these proteins in the same dendrites (Fig. 6) (*30*).

Visualization of NR2B transport by KIF17. Native vesicles, purified from brain with anti-KIF17 beads, moved in a plus-end–directed manner on microtubules when incubated with full-length KIF17 (1–1038) (Fig. 7, A and B) (*31*). Recombinant KIF17 (1–938), lacking the mLin-10 interaction domain, could not move these vesicles on microtubules, and only Brownian movement of the vesicles in the buffer was observed. Because this deletion mutant has motor activity

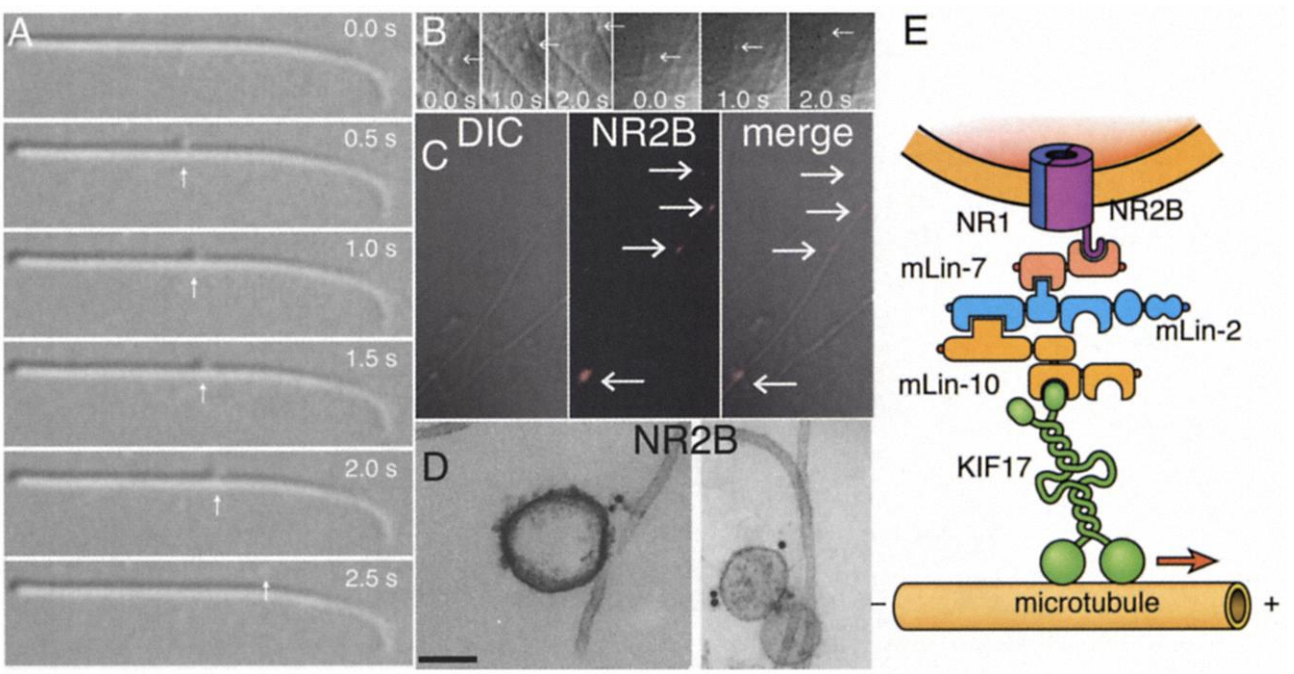

Fig. 7. Visualization of NR2B transport by KIF17. (**A**) Movement of the KIF17 cargo vesicle on axoneme shows plus end–directed motility. Arrow shows the vesicle, which touches on the microtubule and moves, then goes out. [A quicktime movie can be viewed at http://cb.m.u-tokyo.ac.jp/~setou/). (**B**) Two sequences of time-lapse images of movement of the KIF17 cargo vesicles on microtubules. (**C**) Immunofluorescent detection of NR2B on the vesicles moved by KIF17 on microtubules. (**D**) Electron micrograph showing immunocytochemistry of the KIF17-bearing vesicles on a microtubule. NR2B is detected by gold particles (diameter 10 nm). Scale bar, 100 nm. (**E**) Model of the NR2B transporting machinery.

in the microtubule gliding assay (*14*) and vesicles were being released (*31*), it appears that the mLin-10 binding site is necessary for KIF17 to transport these vesicles. Direct fixation and immunodetection by fluorescence in light microscopy (Fig. 7C) and gold labeling in electron microscopy (Fig. 7D) revealed that NR2B is on these active vesicles. Thus, cargoes containing NR2B are transported by KIF17, and the mLin-10 binding tail is necessary for this function of KIF17.

These data collectively suggest that KIF17, a neuron-specific molecular motor with microtubule plus-end–directed motility interacts directly with a mLin-10 PDZ domain, resulting in the transport of NR2B in dendrites. We propose this motor-cargo complex as the sorting machinery for NR2B.

References and Notes

1. R. S. Petralia, Y. X. Wang, R. J. Wenthold, *J. Neurosci.* **14**, 6102 (1994); M. E. Rubio and R. J. Wenthold, *Neuron* **18**, 939 (1997); *J. Neurosci.* **19**, 5549 (1999); S. J. Smith, *Science* **283**, 1860 (1999).
2. M. D. Ehlers, A. L. Mammen, L. F. Lau, R. L. Huganir, *Curr. Opin. Cell Biol.* **8**, 484 (1996); M. Sheng and E. Kim, *Curr. Opin. Neurobiol.* **6**, 602 (1996); M. B. Kennedy, *Trends Neurosci.* **20**, 264 (1997).
3. N. Hirokawa, *Science* **279**, 519 (1998); D. L. Foletti, R. Prekeris, R. H. Scheller, *Neuron* **23**, 641(1999).
4. T. Nakagawa *et al.*, *Proc. Natl. Acad. Sci. U.S.A.* **94**, 9654 (1997).
5. Z. Songyang *et al.*, *Science* **275**, 73 (1997).
6. J. S. Simske, S. M. Kaech, S. A. Harp, S. K. Kim, *Cell* **85**, 195 (1996); D. S. Bredt, *Cell* **94**, 691 (1998); S. Butz, M. Okamoto, T. C. Südhof, *Cell* **94**, 773 (1998); J. P. Borg *et al.*, *J. Biol. Chem.* **273**, 31633 (1998); S. M. Kaech, C. W. Whitfield, S. K. Kim, *Cell* **94**, 761 (1998).
7. K. Moriyoshi *et al.*, *Nature* **354**, 31 (1991); H. Meguro *et al.*, *Nature* **357**, 70 (1992); M. Sheng *et al.*, *Nature* **368**, 144 (1994)
8. Eleven independent clones were obtained from a 4-week-old mouse brain cDNA library that was probed with the motor domain. Northern blot analysis with a motor domain probe detected 5-kb KIF17 mRNA bands in brain and a 3-kb band in the testes, which could be an alternative splice short variant of KIF17.
9. M. A. Shakir, T. Fukushige, H. Yasuda, J. Miwa, S. S. Siddiqui, *Neuroreport* **4**, 891 (1993); M. Tabish, Z. K. Siddiqui, K. Nishikawa, S. S. Siddiqui, *J. Mol. Biol.* **247**, 377 (1995).
10. Phylogenetic tree, sequence comparison, and coiled-coil prediction were analyzed as described (*18*).
11. Antibody (anti-KIF17) was generated against amino acids 505 to 717 of a KIF17 thioredoxin fusion protein (bold italics in Fig. 1A). All the experiments in this article used anti-KIF17 that had been affinity-purified with purified full-length recombinant KIF17 protein (*12*). In Fig. 1E, brain sample [1 μg per lane of the total homogenate in RIPA buffer (50 mM tris, 1% Triton X-100, 0.1% SDS, and 150 mM NaCl, pH 8.0)] was detected with anti-KIF17 that had been biotinylated (biotinylation kit, Pierce) and detected with avidin-ALP (Pierce) according to the manufacturer's instructions; purified recombinant KIF17 (10 μg/ml) was used for the peptide blocking. Anti–mLin-10 was provided by T. Südhof, anti–mLin-7 was provided by Y. Hata (*32*), and anti-NR1 (αGluRζ1 No43), anti-NR2B COOH-terminal peptide (αGluRε No34), and anti-NR2B NH_2-terminal peptide (αGluRε No59) (*33*) were provided by M. Mishina. PSD-95, NR2B, synaptotagmin, mLin-2, and mLin-10 mAbs were purchased from Transduction Laboratory, anti–substance P receptor was from Novus, anti-glycine receptor and NR1 mAb from Chemicon, and anti-GABAARβ2 from Santa Cruz. All the protein detection in immunoprecipitants was confirmed by all available antibodies: anti–mLin-10, NR1 antibodies (αGluRζ1 No43 and NR1 mAb), and NR2B antibodies (αGluRε No34, αGluRε No59, and NR2B mAb). The data shown in Figs. 4 and 5 are mAb blots.
12. NH_2-terminal, His-tagged full-length KIF17-expressing baculovirus was constructed using the Fast-Bac system (Gibco Life Technologies). High-Five cells (Invitrogen) were infected with the virus for 60 hours in Grace Insect Medium (Gibco Life Technologies) and harvested and purified as described (*18*).
13. Supernatant from mouse brain homogenates after centrifugation at 75,000 rpm for 1 hour in a Beckman TL100.3 rotor in HBS (10 mM Hepes, pH 7.4, and 150 mM NaCl) with proteinase inhibitors (1 mM phenylmethyl sulfonyl fluoride, 210 μM leupeptin, 145 μM pepstatin A, 260 μM *N*-α-*p*-tosyl-L-arginine methyl ester hydrochloride, and 10 mM benzamidine) was centrifuged in a Beckman SW28 rotor for the velocity gradient. Gel-filtration assay was with Superose 6 (Amersham Pharmacia Biotech). Native PAGE was done as described (*18*).
14. Axoneme and microtubule motility assay of KIF17 was as described (*18*) with slight modification of the motility buffer (10 mM imidazole, 5 mM $MgCl_2$, 1 mM EGTA, 5 mM dithiothreitol, 5 mM Mg–adenosine triphosphate (ATP), and 50 mM NaCl, pH 7.4). Glass surface with KIF17 tailless construct (1–938) also had similar motility on this assay; KIF17 tailless (1–938) and headless (939–1038) mix had the same activity. These deletion mutants were assayed as a positive control for the vesicle motility assay and competition assay.
15. For tissue distribution analysis, 4-week-old male mouse total homogenate in RIPA was used; 20 μg of protein was loaded per lane. For neuronal distribution analysis, 5 μg of protein was loaded per lane.
16. For immunochemistry, brains from 4-week-old male mice were fixed in 4% paraformaldehyde, 0.1% glutaraldehyde, and 4% sucrose in phosphate-buffered saline (PBS) and slices were prepared as described (*18*). The cultured hippocampal neurons were fixed in 4% paraformaldehyde and permeabilized with 0.1% Triton X-100. The samples were blocked with 10% bovine serum albumin (BSA) and incubated with anti-KIF17 (5 μg/ml) and pNFH mAb (Sigma, 1:1000 dilution) or MAP2 mAb (Sigma, 1:1000 dilution). For controls, preimmune immunoglobulin G (IgG) was used as the first antibody. After overnight incubation at 4°C, the samples were washed with PBS and incubated with Alexa 488–conjugated goat antibody to rabbit IgG and blocked by 10% BSA, Alexa 568–conjugated goat antibody to mouse IgG+H (Molecular Probes, 1:100 dilution). TOTO-3 (Molecular Probes) was used as a nucleotide marker for the triple staining. For double labeling with polyclonal antibodies (Fig. 6, B and C), biotinylated anti-KIF17 (*11*) was used and detected with Alexa 568–streptavidin (Molecular Probes) in accordance with the manufacturer's instructions. The samples were observed under a confocal laser scanning microscope (LSM510, Zeiss).
17. The floating assay and electron microscopy study were performed as described (*18*), with slight modification. The postnuclear supernatant of gray matter in IM-Ac (*18*) buffer was centrifuged with a continuous gradient from 40% to 0% Nycodenz for 4 hours at 65,000 rpm in a Beckman NVTi65 rotor, and 32 fractions were collected. The fraction that contained the highest concentration of KIF17 (26th) (~0.3 ml) was incubated overnight with 1 μg of anti-KIF17 or 1 μg of control preimmune IgG at 4°C and then with 10 μl of second antibody–coated magnetic beads (Dynal) for 12 hours at 4°C. Then the sample was washed five times and processed for further analysis.
18. Y. Okada *et al.*, *Cell* **81**, 769 (1995); N. Saito *et al.*, *Neuron* **18**, 425 (1997).
19. The floated vesicles containing fractions (100 μl) (*17*) were diluted with 1 ml of each buffer and incubated for 10 min with gentle agitation at 4°C, then pelleted by centrifugation at 10,000*g* for 30 min at 4°C. Buffers were as follows: control, IMac [150 mM K-acetate, 50 mM imidazole, 5 mM Mg-acetate, and 1 mM EGTA (pH 7.4)]; high salt, IMAc with 0.5 M KCl; high pH, 0.1 M Na_2CO_3 (pH 11.5).
20. Yeast two-hybrid screening and assays were performed as described in the Clontech standard protocol with the EGY48 yeast strain harboring Leu2 and β-galactosidase as reporter genes. KIF17 939–1038 was subcloned into pLexA (LexA fusion vector) and used to screen ~10^7 clones from mouse brain cDNA libraries constructed in pB42AD (GAL1 activation domain vector, Clontech). We selected 20 Leu^+/$LacZ^+$ colonies. Two colonies encoded fragments of *mLin-10* gene (457–840), which codes for a portion 99% identical to the corresponding portion of rat Lin-10 (Mint1). cDNA segments were amplified by the polymerase chain reaction (PCR) with specific primers and subcloned into pLexA or pB42AD.
21. Purified GST-fused COOH-terminus of KIF17 (939–1038) was immobilized on a BIACore CM5 sensor chip, equilibrated with 50 mM Hepes-NaOH (pH 8.0) containing 100 mM NaCl, and superfused with purified mLin-10 (650-840 with His6 on NH2-terminal) at a flow rate of 10 μl/min. Binding activities (in resonance units) were measured as the difference between the baseline value determined 20 s before sample injection and the measurements taken at the indicated time points. All experiments were performed at 25°C with BIACORE3000. Data were analyzed with the BIA evaluation program, version 3.0 [BIACORE; M. Irie *et al.*, *Science* **277**, 1511 (1997)].
22. A pull-down assay was performed with the postnuclear supernatant obtained from 2-week-old mouse brain lysates in HBST [10 mM Hepes (pH 7.4), 150 mM NaCl, 0.1% Triton X-100, and proteinase inhibitors] and 10 μg of immobilized GST fusion KIF17 tail region recombinant protein or 10 μg of KIFC2 1–433 protein. After 12 hours of incubation, the beads were washed five times and immunoblotted with anti–mLin-10. Recombinant proteins were expressed in *E. coli* strain BL21(DE3) (Stratagene) with the pGEX vector (Amersham Pharmacia Biotech) and purified by 10 μl of Glutathione Sepharose Fast Flow (Amersham Pharmacia Biotech).
23. Four-week-old male mouse brains were dissected as reported (*18*) in HBST buffer. Lysates of the brains (0.5 ml) were incubated with 20 μl of anti–mLin-10 serum and 10 μl of protein A–Sepharose Fast Flow (Amersham Pharmacia Biotech) overnight at 4°C and were washed five times with 0.5 ml of HBST. Sample was loaded at 5 μl per lane. Control is that of normal rabbit IgG.
24. K. Jo, R. Derin, M. Li, D. S. Bredt, *J. Neurosci.* **19**, 4189 (1999).
25. Total homogenate of brain, prepared from 11-day post coitum embryo to 3-week-old postnate, was loaded at 20 μg per lane on SDS-PAGE, and each protein was detected by Western blotting.
26. The figure shows the fractions of the floating assay (*17*).
27. A 4-week-old male mouse brain was dissected for use as reported (*18*) in HBST buffer. Lysates of the brains (0.5 ml) were incubated with 20 μl of anti-KIF17 serum and 10 μl of protein A–Sepharose Fast Flow at 4°C overnight and were washed five times with 0.5 ml of HBST. Sample was loaded at 5 μl per lane. The NR2B was solubilized ~5% in 0.1% Triton, ~5% in RIPA, and ~30% in 1% deoxycholate (Doc) (*28*). The amount of immunoprecipitated NR2B by KIF17 is ~5% of the lysates in 0.1% Triton, ~5% in RIPA, and less in 1% Doc (*28*). There may be at least two populations of NR2B, with one population incorporated and anchored at the postsynaptic sites, and the other in the vesicles in the cytoplasm (some of which are transported by KIF17, forming complex with mLin-10, mLin-7, and mLin-2). Our immunofluorescence study indicates that strong permeabilization preserves synaptic NMDA receptors but affects the localization of cytoplasmic NMDA receptors, which suggests that strong detergent treatment affects the preservation of cytoplasmic NMDA receptors (*28*). From these results, we chose 0.1% Triton in this study.
28. M. Setou and N. Hirokawa, unpublished data; J. Blahos II and R. J. Wenthold, *J. Biol. Chem.* **271**, 15669 (1996).
29. Vesicle immunoprecipitation was done as described (*18*). Extra bands on KIF1A immunoprecipitation products are degradates that appear after incubation. Cover glass chambers (10 μl) coated with microtubules and blocked with BSA (2 mg/ml) were incubated with the floated fraction added with 5 mM ad-

enylyl-imidodiphosphate (AMP-PNP) or ATP and 10 μM taxol at 27°C for 10 min, washed by each buffer, and processed for immunodetection (*16*). The vesicles on microtubules were observed in differential interference contrast laser scanning microscope (DIC-LSM). For the blocking assay, KIF17 tail peptide (GST-KIF17 939–1038) (*22*) was incubated with the floated vesicles for 6 hours before the microtubule binding assay. The total concentration of protein was equalized by addition of GST alone.

30. Mouse hippocampal neurons were fixed in 4% paraformaldehyde (PFA) and permeabilized with 0.1% Triton X-100 for 3 min. The brain sections were fixed in 4% PFA. For NR2B staining of the sections, pepsin treatment was performed as described (*33*). Anti-NR1 (αGluRζ1 No43) and NR1 mAb, anti-NR2B COOH-terminal peptide (αGluRε No34), and anti-NR2B NH_2-terminal peptide (αGluRε No59) each gave the same results.
31. For this experiment, we first purified KIF17-bearing membrane organelles from KIF17-enriched fractions of floating assay (*14*). Anti-KIF17–coated beads with vesicles attached (5 μl) were incubated for 1 hour in three different conditions: (i) 30 μl of recombinant full-length KIF17 (1 mg/ml), (ii) recombinant tailless KIF17 (1–938) (1 mg/ml), and (iii) tail-deleted construct (1–938) (0.8 mg/ml) mixed with tail construct (GST-KIF17 939–1038) (0.2 mg/ml) (*22*). Through this process, KIF17 vesicles were detached from beads. In the third condition, tail construct was added to exclude the possible difference of detachment of the vesicles from the beads. Then, eluted supernatant was diluted in 100 μl of motility buffer (*14*) and placed in the observation chamber. In all three conditions, Brownian movement of the detached vesicles was observed. In the first condition, almost all (more than 10 movements in 3 min of observation) of the vesicles that were in contact with axoneme moved. No vesicle movement on axoneme was observed in the other two conditions. Identification of vesicles correlated with motility as described (*34*). Of the vesicles attached to microtubules by KIF17, ~40% were $NR2B^+$. NR2B was not detected in the vesicles isolated with anti-KIF3B immunobeads as a control.
32. M. Irie *et al.*, *Oncogene* **18**, 2811 (1999).
33. M. Watanabe *et al.*, *Eur. J. Neurosci.* **10**, 478 (1998); T. Kutsuwada *et al.*, *Neuron* **16**, 333 (1996); H. Mori *et al.*, *Neuron* **21**, 571 (1998).
34. J. Taunton *et al.*, *J. Cell Biol.* **148**, 519 (2000).
35. We thank T. Südhof for anti–mLin-10; Y. Hata for anti–mLin-7; M. Mishina for the anti-NR subunits; M. Watanabe, M. Mishina, T. Takahashi, T. Nakata, and Y. Kanai for discussions and advice; K. Yamamoto, L. Guillaud, Y. Ikeda, Y. Okada, M. Kikkawa, S. Nonaka, H. Sato, H. Fukuda, and M. Sugaya for technical assistance; and other members of the Hirokawa lab for technical assistance, stimulating discussions, and valuable advice throughout. Supported by the Japanese Society for Promotion of Science Research Fellowship for Young Scientists (T.N. and D.-H.S.) and by a Special Grant-in-Aid for Center of Excellence from the Japan Ministry of Education, Science, Sports and Culture (N.H.).

28 December 1999; accepted 17 April 2000

REPORTS

Forming Supramolecular Networks from Nanoscale Rods in Binary, Phase-Separating Mixtures

Gongwen Peng,[1] Feng Qiu,[1] Valeriy V. Ginzburg,[1] David Jasnow,[2] Anna C. Balazs[1]*

Simulations show that when low-volume fractions of nanoscale rods are immersed in a binary, phase-separating blend, the rods self-assemble into needle-like, percolating networks. The interconnected network arises through the dynamic interplay of phase-separation between the fluids, through preferential adsorption of the minority component onto the mobile rods, and through rod-rod repulsion. Such cooperative effects provide a means of manipulating the motion of nanoscopic objects and directing their association into supramolecular structures. Increasing the rod concentration beyond the effective percolation threshold drives the system to self-assemble into a lamellar morphology, with layers of wetted rods alternating with layers of the majority-component fluid. This approach can potentially yield organic/inorganic composites that are ordered on nanometer scales and exhibit electrical or structural integrity.

Dispersion of solid nanoparticles throughout a polymer blend can dramatically improve the mechanical, thermal, or electrical properties of the mixture (*1*). Controlling the distribution of particles within multicomponent polymeric blends, however, remains a considerable challenge. Most polymer pairs are immiscible, and thus, blends usually phase-separate. Typically, one or more of the polymers preferentially adsorb onto the mobile particles. Thus, the motion of the particles influences the behavior of the immiscible polymeric fluids, and the structural evolution of the fluids in turn affects the dispersion of the particles (*2*). The situation becomes even more complex if these particles are rod-like (such as nanotubes or rigid fibers) because rods can form liquid crystalline phases (*3, 4*). Now, interplay among three phenomena—phase-separation, wetting, and anisotropic interparticle interactions—controls the structure of the composite.

We probed these interactions in binary fluid/rod mixtures through computer simulations and show that the irreversible evolution of phase-separating fluids can be exploited to drive the self-assembly of nanoscopic rods into supramolecular networks. Applied to nanotubes, this approach could produce electrically conducting pathways in insulating materials; applied to short, inorganic fibers, the scheme could yield continuous reinforcing structures in organic/inorganic composites. Overall, the results facilitate the efficient fabrication of advanced hybrid materials.

Our two-dimensional simulation combines a coarse-grained description of the binary fluids with a discrete model for solid additives (*5–9*). The binary system is described by a continuous order parameter $\psi(\mathbf{r})$, which is the difference between the local volume fractions of components A and B, $\psi(\mathbf{r}) = \phi_A(\mathbf{r}) - \phi_B(\mathbf{r})$. The flux of ψ is proportional to the local gradient of the chemical potential, which in turn is proportional to the derivative of the free energy, F, with respect to the order parameter

$$\partial\psi/\partial t = \Gamma\nabla^2(\delta F\{\psi\}/\delta\psi) \quad (1)$$

where Γ is the order parameter mobility. The rigid rods are described by discrete entities, each of which has a center-of-mass position $\mathbf{r}_i$ and an orientation angle θ_i measured from a fixed direction. The variables $\mathbf{r}_i$ and θ_i obey Langevin equations

$$\partial\mathbf{r}_i/\partial t = -M\partial F/\partial\mathbf{r}_i + \eta_i \quad (2)$$

$$\partial\theta_i/\partial t = -M'\partial F/\partial\theta_i + \zeta_i \quad (3)$$

where M and M′ are mobility constants, and η_i, and ζ_i are thermal fluctuations that satisfy the fluctuation-dissipation relations. Equations 1 to 3 are discretized and numerically integrated on a 256 by 256 square lattice, which has periodic boundary conditions in both the x and y directions. The lattice sets the unit of length.

[1]Chemical Engineering Department and [2]Department of Physics and Astronomy, University of Pittsburgh, Pittsburgh, PA 15261, USA.

*To whom correspondence should be addressed. E-mail: balazs@vms.cis.pitt.edu